Ablative thermal protection system under uncertainties including pyrolysis gas composition

Mickael Rivier, Jean Lachaud, Pietro Marco Congedo

Ablative thermal protection system under uncertainties including pyrolysis gas composition

Mickaël Rivier, Jean Lachaud , Pietro Marco Congedo

Ablative thermal protection system under uncertainties including pyrolysis gas composition

Mickaël Rivier[*][†], Jean Lachaud [‡], Pietro Marco Congedo [§]

Project-Teams CARDAMOM

Abstract: Spacecrafts such as Stardust (NASA, 2006) are protected by an ablative Thermal Protection System (TPS) for their hypersonic atmospheric entry. A new generation of TPS material, called Phenolic Impregnated Carbon Ablator (PICA), has been introduced with the Stardust mission. This new generation of low density carbon-phenolic composites is now widely used in the aerospace industry. Complex heat and mass transfer phenomena coupled to phenolic pyrolysis and pyrolysis gas chemistry occur in the material during atmospheric entry. Computer programs, as the Porous material Analysis Toolbox based on OpenFoam (PATO) released open source by NASA, allow to study the material response. In this study, a non-intrusive Anchored Analysis of Variance (Anchored-ANOVA) method has been interfaced with PATO to perform low-cost sensitivity analysis on this problem featuring a large number of uncertain parameters. Then, a Polynomial-Chaos method has been employed in order to compute the statistics of some quantities of interest for the atmospheric entry of the Stardust capsule, by taking into account uncertainties on effective material properties and pyrolysis gas composition. This first study including pyrolysis gas composition uncertainties shows their key contribution to the variability of the quantities of interest.

Key-words: Sensitivity analysis, Uncertainty quantification, Porous media, Heat-shield ablation

[*] Inria Bordeaux Sud-Ouest - Team CARDAMOM
[†] ArianeGroup, Le Haillan
[‡] C la Vie, University of New Caledonia, New Caledonia
[§] DeFI - CMAP - Ecole Polytechnique, Inria Saclay - Ile de France, Polytechnique - X, CNRS

Système de protection thermique ablatif sous incertitudes avec prise en compte des gazs de pyrolyse

Résumé : Les véhicules spaciaux tels que Stardust (NASA, 2006) sont protégés par un système de protection thermique ablatif (TPS) lors de leur entrée atmosphérique hypersonique. Une nouvelle génération de matériau de protection, appelé Phenolic Impregnated Carbon Ablator (PICA), a été introduite pour la mission Stardust. Cette nouvelle génération de composites carbone-phénolique à faible densité est maintenant couramment utilisée dans l'industrie aérospatiale. Les phénomènes complexes de transfert de masse et de chaleur couplés à la pyrolyse de la matrice phénolique et la chimie des gaz associés surviennent dans le matériau durant l'entrée atmoshpérique. Différents codes de calcul, comme Porous material Analysis Toolbox based on OpenFoam (PATO) mis en accès libre par la NASA, permettent d'étudier la réponse du matériau. Dans notre étude, une méthode non-intrusive Anchored Analysis of Variance (Anchored-ANOVA) a été interfacée avec PATO pour réaliser une analyse de sensibilité à faible coût sur ce problème comportant un grand nombre de parmètres incertains. Ensuite, une méthode de chaos polynomial a été mise en oeuvre afin de calculer les statistiques de différentes quantités d'intérêt lors de l'entrée atmosphérique de la capsule Stardust, en considérant les incertitudes sur les propriétés matériau et la composition des gaz de pyrolyse. Cette première étude prenant en compte les incertitudes sur la composition des gaz de pyrolyse montre leur forte contribution à la variabilité finale des quantités d'intérêt.

Mots-clés : Analyse de sensibilité, Quantification des incertitudes, Milieu poreux, Abalation de bouclier thermique

1 Introduction

Space exploration missions often include entering a planetary atmosphere at hypersonic speed. A high enthalpy hypersonic shock forms around the spacecraft and kinetic energy is progressively dissipated into heat [1]. Heat is transferred to the surface of the spacecraft by radiation and convection. A suitable heat shield is needed to protect the payload. The level of heat flux increases with entry speed and atmospheric density. For fast hypersonic entries, typically faster than $8\,km/s$ from earth orbit, ablative materials are used as Thermal Protection Systems (TPS). These materials mitigate the incoming heat through phase changes, chemical reactions, and material removal [2]. A low-density porous carbon/phenolic composite called PICA was used for the Stardust comet-dust sample-return capsule, which reentered the Earth's atmosphere at $12.7\,km/s$ [3]. PICA is made of a carbon fiber preform partially impregnated with phenolic resin.
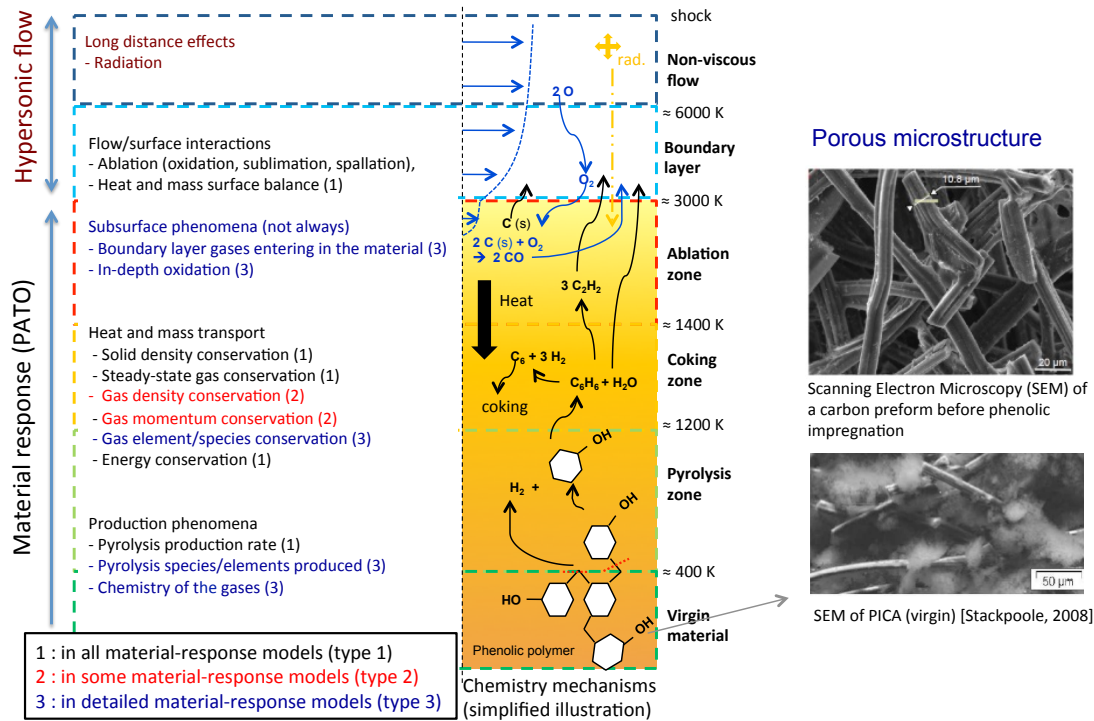
Figure 1: Phenomenology of porous carbon/phenolic ablative materials

During atmospheric entry, carbon/phenolic materials undergo thermal degradation and ultimately recession captured by the following physico-chemical phenomena (Figure 1). The phenolic polymer thermally decomposes and progressively carbonizes into a low density carbon form, losing mass while releasing pyrolysis gases. The pyrolysis gases percolate and diffuse to the surface through the network of pores. Reactions within the pyrolysis-gas mixture (homogeneous reactions) and between pyrolysis gases and the char take place with possible coking effects (heterogeneous reactions). Mixing and reaction of the pyrolysis gases with boundary layer gases into the pores of the material occur when boundary layer gases penetrate in the material by forced

convection or due to fast diffusion at low pressures [4]. At the surface, the material is removed by ablation and the outer surface recedes. Depending on entry conditions, ablation may be caused by heterogeneous chemical reactions (oxidation, nitridation), phase change (sublimation), and possibly mechanical erosion (often called spallation).

A detailed heat and mass transfer model is required to estimate the performance of the porous material and design the thermal protection system. Two important design criteria are the expected level of recession and the maximum back wall temperature. The key parameter uncertainties are propagated to obtain the design uncertainties to be used in the margin policy [5]. A Monte Carlo approach has been developed and used to propagate uncertainties on material properties and areoheating conditions for the design of the NASA Mars Science Laboratory [6] and Orion [7] spacecrafts. In these study however, no uncertainty is attributed to the pyrolysis gas composition. Recent publications have shown that the pyrolysis gas composition strongly varies depending on temperature and heating rate [8, 9, 10]. The pyrolysis gases are composed of carbon, oxygen and hydrogen elements. The pyrolysis gas composition influences the pyrolysis gas enthalpy - which impacts heat transfer in the porous material - and the boundary layer chemistry - which controls the ablation rates and the surface temperature. For this first analysis we will allow an uncertainty of 10% on these elements. The composition in term of species is then computed in each cell of the mesh and at each time step using an equilibrium chemistry solver [4]. This makes the computation very costly and requires the use of the low-cost uncertainty quantification methods. In the literature, low-cost uncertainty propagation has been already performed alongside Global Sensitivity Analysis for problems of natural convection in [11]. Uncertainty analyses have also been performed on surface ablation rates and their effect on aeroheating predictions for Mars entry in [12], and on ablation problems in plasma wind tunnel [13, 14].

In section 2, we present the problem studied and the physical hypotheses. In section 3, we present the inverse analysis method implemented in the study. The results of the uncertainty quantification analysis are presented in section 4. Finally, section 5 draws some conclusions and perspectives.

2   Definition of the uncertainty analysis problem and hypotheses

For this first analysis, we chose to study the entry of Stardust, that was the first mission using a low-density carbon-phenolic ablator in 2006. The thermal response of the TPS has been be studied at the stagnation point during the whole reentry, from entry interface to cool down. As in the state-of-the-art design approach we assumed that the problem is locally mono-dimensional. The actual thickness of the ablative material was two inches [3], therefore we used this value. Adiabatic conditions are used at the bondline. A convective boundary condition is used at the surface of the ablative material. Surface total pressure and heat flux were taken from reference [15].

Figure 2 illustrates the temperature evolution during the atmospheric entry at the stagnation point and in-depth under the stagnation point with nominal TACOT properties.

The analysis is performed using the properties of the Theoretical Ablative Composite for Open Testing (TACOT). Its composition and properties are comparable to PICA. Nominal TACOT properties are available in the open literature [16]. Volume-wise, TACOT is made of 10% of carbon fibers, 10% of phenolic resin, and is 80% porous.
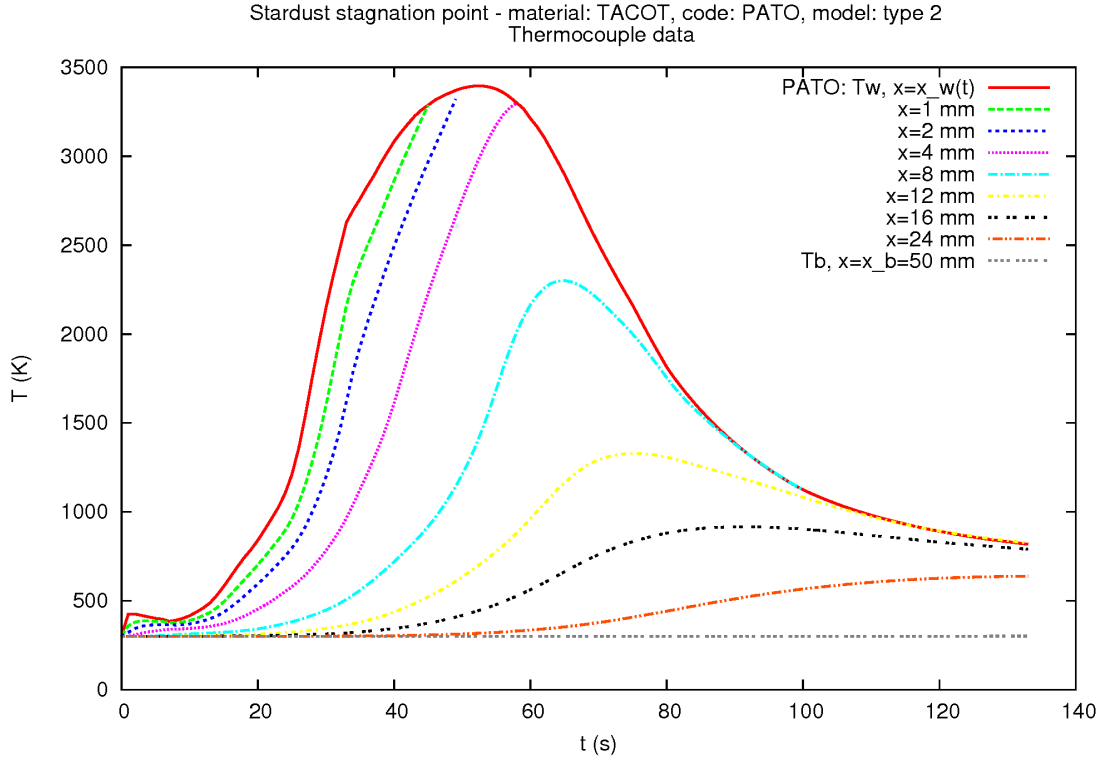
Figure 2: Surface and in-depth temperatures obtained with nominal material and pyrolysis gas composition parameters.

2.1 Model

A generic heat and mass transfer model for porous media has been recently developed and documented [17]. It is suitable to model ablative heat shields. For the sake of conciseness, we only present a short summary in this section. The model was developed for porous materials containing several solid phases and a single gas phase. The detailed chemical interactions occurring between the solid phases and the gas phase are modeled at the pore scale assuming local thermal equilibrium. Homogenized models were obtained for solid pyrolysis, pyrolysis species injection in the gas phase, heterogeneous reactions between the solid phases and the gas phase, and homogeneous reactions in the gas phase. The chemistry models were integrated in a macroscopic model making use of volume-averaged governing equations for the conservation of solid mass, gas mass, species (finite-rate chemistry) or elements (equilibrium chemistry), momentum, and energy. The model is implemented in the Porous material Analysis Toolbox (PATO), distributed Open Source by NASA. First-order implicit finite-volume schemes in time and space [18, 19], which have been shown to provide excellent convergence and accuracy [20, 4], were used for the simulations presented in Section 4. In this study, we used an equilibrium chemistry model that is equivalent to the reference NASA TPS design model [21]. The current approach is to assume that the elemental pyrolysis gas composition is fixed. To save on computational time, precomputed tables are used to obtain the gas composition (species) and properties (enthalpy, viscosity,

molar mass). In the current study, we wish to vary the elemental pyrolysis gas composition. The pyrolysis gas composition in term of species is therefore computed from pyrolysis gas elemental composition in each cell of the mesh and at each time step using an equilibrium chemistry solver, as described in [4]. The surface ablation rate is computed using the thin film coefficient approach, also known as B' approach, accounting for the change in pyrolysis gas composition injected in the boundary layer [4].

2.2 Uncertain parameters and associated uncertainties

In previous studies, uncertain material property parameters have been identified for PICA [6, 5, 22]. We decided to include the same uncertain parameters in our study. We also added a set of new parameters to assess the effect of the pyrolysis gas composition on the material response as described in the introduction. The nominal elemental composition of the pyrolysis gases for TACOT are, in mole fractions, C (0.206), H (0.679), O (0.115). In total, we have used twenty-seven uncertain parameters in the TACOT material model. We have attributed 5 to 10 % uncertainty to each of them as follows (the number in brackets is the label used to identify each uncertainty in the following of this paper):

- Density (1) and volume fraction (2) of the fibrous preform (5% uncertainty),

- Density (3) and volume fraction (4) of the phenolic matrix (5% uncertainty),

- Virgin's (5) and char's (6) permeability (5% uncertainty),

- Pyrolysis model (10% uncertainty):

    - Elementary composition of the pyrolysis gases in Carbon (7) , Hydrogen (8) and Oxygen (9),
    - Pyrolysis reaction 1: pre-exponential factor (10), activation energy (11), pyrolysis enthalpy (12),
    - Pyrolysis reaction 2: pre-exponential factor (13), activation energy (14), pyrolysis enthalpy (15),

- Thermal properties of virgin material (5% uncertainty): heat capacity (16), orthogonal conductivity (17), radial conductivities (18, 19), emissivity (20), reflectivity (21),

- Thermal properties of charred material (5% uncertainty): heat capacity (22), orthogonal conductivity (23), radial conductivities (24, 25), emissivity (26), reflectivity (27).

We chose to simplify the constraint of elementary fractions summing to one through maintaining the relative ratios and normalizing the elementary composition. Practically, given a random draw of the mass fractions y_i within the $\pm 10\%$ interval, normalized mass fractions $\widetilde{y}_i = \dfrac{y_i}{\sum\limits_k y_k}$

will actually be given to PATO.

Moreover, with ϵ_1 and ϵ_2 the uncertain volume fraction of the fibrous preform and the virgin matrix respectively, the virgin and charred porosities ε_v and ε_c are computed as follows:

$$\varepsilon_v = 1 - \epsilon_1 - \epsilon_2$$
$$\varepsilon_c = 1 - \epsilon_1 - \frac{\epsilon_2}{2}$$

Finally, one may note the presence of 3D conductivities in the list of uncertain parameters, which clashes with the mono-dimensional assumption made earlier. Such parameters are left in

the study to artificially increase the input dimension and verify the capability of the proposed approach to detect their null impact and discard them.

3   Sensitivity and uncertainty analysis theory and tools

Let us consider a stochastic differential equation of the form:

$$L\left(\mathbf{x}, \boldsymbol{\xi}, \phi\right) = f\left(\mathbf{x}, \boldsymbol{\xi}\right) \tag{1}$$

where L is a non-linear spatial differential operator (for instance, the steady Navier-Stokes operator) depending on a set of uncertainties, designated with the random vector $\boldsymbol{\xi}$ (of dimension the number of uncertain parameters in the problem) and where $f(\mathbf{x}, \boldsymbol{\xi})$ is a source term depending on $\mathbf{x}$ and $\boldsymbol{\xi}$. In the following, we drop the dependence on $\mathbf{x}$ in order to simplify the notation. The solution of the stochastic equation (1) is $\phi(\boldsymbol{\xi})$, which is a function of the space variable $\mathbf{x} \in \mathbb{R}^d$ and of $\boldsymbol{\xi} \in \Xi = \Xi_1 \times \cdots \times \Xi_N$ ($\Xi \subset \mathbb{R}^N$) and $\boldsymbol{\xi} \in \Xi \longmapsto \phi(\boldsymbol{\xi}) \in L^2(\Xi, p(\boldsymbol{\xi}))$, where $p(\boldsymbol{\xi}) = \prod_{i=1}^N p(\xi_i)$ is the probability density function of $\boldsymbol{\xi}$.

One of the objective of Uncertainty Quantification is to compute the statistics of the quantity of interest, *i.e.* $\phi(\boldsymbol{\xi})$.

We can define the central statistical moment of ϕ of order n as

$$\mu^n(f) = \int_\Xi \left(\phi(\boldsymbol{\xi}) - E(\phi)\right)^n p(\boldsymbol{\xi}) \mathrm{d}\xi, \tag{2}$$

where $E(\phi)$ indicates the expected value of ϕ

$$E(\phi) = \int_\Xi \phi(\boldsymbol{\xi}) p(\boldsymbol{\xi}) \mathrm{d}\xi. \tag{3}$$

In the following, we indicate with σ^2, the variance (second-order moment). We illustrate the main concepts of the ANOVA-decomposition in Section 3.1. Then, to clearly present the context of uncertainty analysis theory and provide a comprehensive understanding of the approach followed in this work, we will use as illustration a mono-dimensional heat transfer problem presented in Section 3.2. The UQ methods are then described in Section 3.3.

3.1   ANOVA-based decomposition

Let us suppose that the response of a given system of interest can be represented by a $N-$dimensional function:

$$y = \phi(\boldsymbol{\xi}) = \phi(\boldsymbol{\xi}_1, \boldsymbol{\xi}_2, \cdots, \boldsymbol{\xi}_N) \tag{4}$$

We consider Eq. (4) in its functional expansion form as follows

$$y = \phi_0 + \sum_{1 \leqslant i \leqslant N}^N \phi_i(\boldsymbol{\xi}_i) + \sum_{1 \leqslant i < j \leqslant N}^N \phi_{ij}(\boldsymbol{\xi}_i, \boldsymbol{\xi}_j) + \cdots + \phi_{1,2,\cdots,N}(\boldsymbol{\xi}_1, \boldsymbol{\xi}_2, \cdots, \boldsymbol{\xi}_N)$$

or in compact form using a multi index system:

$$y = \phi_{s_0} + \sum_{j=1}^{2^N - 1} \phi_{s_j}(\boldsymbol{\xi}_{s_j}) \tag{5}$$

The multi indices s_j are defined such as

$$
\begin{array}{rcl}
s_0 & = & (0,0,0,\cdots,0) \\
s_1 & = & (1,0,0,\cdots,0) \\
s_2 & = & (0,1,0,\cdots,0) \\
& \vdots & \\
s_N & = & (0,0,0,\cdots,1) \\
s_{N+1} & = & (1,1,0,\cdots,0) \\
s_{N+2} & = & (1,0,1,\cdots,0) \\
& \vdots & \\
s_{\mathcal{N}} & = & (1,1,1,\cdots,1)
\end{array}
\tag{6}
$$

where $\mathcal{N} = 2^N - 1$. The representation of Eq. (5) is called ANOVA (Analysis Of Variance) decomposition [23] of $\phi(\boldsymbol{\xi})$, if for any $j \in \{1, \cdots, \mathcal{N}\}$,

$$
\int_{\mathbb{R}} \phi_{s_j}(\boldsymbol{\xi}_{s_j}) p(\boldsymbol{\xi}_i) \, \mathrm{d}\boldsymbol{\xi}_i = 0 \quad \text{for} \quad \boldsymbol{\xi}_i \in \{\boldsymbol{\xi}_{s_j}\}
\tag{7}
$$

It follows from Eq. (7) the orthogonality of ANOVA component terms, namely

$$
E(\phi_{s_j} \phi_{s_k}) = 0 \quad \text{for} \quad j \neq k
\tag{8}
$$

ANOVA allows identifying the contribution of a given stochastic parameter to the total variance of an output quantity. Meanwhile, we obviously have

$$
E(\phi_{s_j}) = 0 \quad \text{for} \quad j = 1, \cdots, \mathcal{N}
$$

Note that the terms in the ANOVA decomposition can be expressed as integrals of $\phi(\boldsymbol{\xi})$. Indeed, we have

$$
\begin{array}{rcl}
E(Y) & = & \phi_0 \\
E(Y|\boldsymbol{\xi}_i) & = & \phi_0 + \phi_i(\boldsymbol{\xi}_i) \\
E(Y|\boldsymbol{\xi}_i, \boldsymbol{\xi}_j) & = & \phi_0 + \phi_i(\boldsymbol{\xi}_i) + \phi_j(\boldsymbol{\xi}_j) + \phi_{ij}(\boldsymbol{\xi}_i, \boldsymbol{\xi}_j)
\end{array}
\tag{9}
$$

and so on, where $E(Y|\cdot)$ denotes the conditional expectation.

3.2 Analytical solution for transient heat transfer

3.2.1 Deterministic problem

Effective heat transfer is the main mode of energy transport in most porous materials. Let us consider a homogeneous semi-infinite unidimensional medium. Under the assumption of constant material properties, the transient heat transfer equation is given by

$$
\partial_{\mathbf{t}} T = \alpha \, \partial_{\mathbf{x}}^{\mathbf{2}} T
\tag{10}
$$

where $\alpha = k/(\rho \times c_p)$ is the diffusivity. We will consider a medium initially at the room temperature $T(x, t=0) = T_0 = 300$ K. Its surface temperature is held at $T(x=0, t) = T_w = 1646$ K during the experiment. Laplace transform is used for its resolution as presented in Appendix A. The temperature profile as a function of time and space is given by

$$
T(x,t) = T_0 + (T_w - T_0) \, \mathbf{erfc}\left(\frac{x}{2\sqrt{\alpha t}}\right)
\tag{11}
$$

where **erfc** is the complementary error function. The temperature profiles computed for times of 1, 10 and 60 seconds are plotted in Fig. 3 for a representative medium of diffusivity of 10^{-7} m^2/s. We will only consider in the illustrations that follow the first centimeter of the medium. We see here that the hypothesis that the medium is semi-infinite does not play a role on the result, as the heat wave hasn't reached the one centimeter mark after one minute of heating.
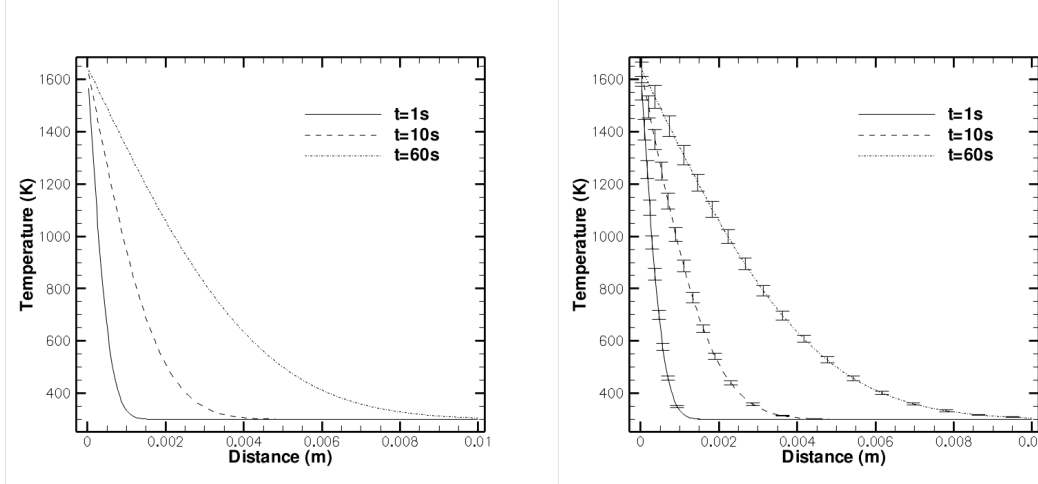

Figure 3: Analytical solution for unidimensional transient heat transfer with fixed surface temperature, for a semi-infinite medium of thermal diffusivity 10^{-7} m^2/s. Initial temperature of the body: 300 K; surface temperature: 1646 K. Left: temperature profiles for 1, 10, and 60 seconds. Right: error bars in terms of standard deviation when considering two uncertainties.

3.2.2 Formulation under uncertainty

Let us now formulate the problem presented in Eq. 10 under an uncertainty quantification perspective. In particular, let assume that two parameters are affected by some variability and/or are not well-known: a 5% of variation in terms of min/max is then imposed on T_w and α considering a uniform distribution (with respect to the deterministic values previously used, denoted in the following as T_{wm} and α_m, respectively). The problem is now formulated as follows:

$$\partial_{\mathbf{t}} T = \alpha \, \partial_{\mathbf{x}}^{\mathbf{2}} T = \alpha_m \times (0.95 + (1.05 - 0.95) * \boldsymbol{\xi}_2) \, \partial_{\mathbf{x}}^{\mathbf{2}} T \tag{12}$$

where $T_w = T_{wm} \times (0.95 + (1.05 - 0.95) * \boldsymbol{\xi}_1)$, and $\boldsymbol{\xi}_1, \boldsymbol{\xi}_2$ vary in $[0, 1]$.

Several methods can be used in order to solve the problem defined in Eq. 12. In this work, we use systematically the so-called non-intrusive methods: this means that a single deterministic computation (used to solve for example the differential operator defined in Eq. 10) is replaced with a whole set of such computations, each one of those being run for specific values of the uncertain conditions. The final solution can be then written as follows:

$$T(x, t, \boldsymbol{\xi}_1, \boldsymbol{\xi}_2) = T_0 + (T_{wm}(0.95 + 0.1\boldsymbol{\xi}_1) - T_0) \, \mathbf{erfc} \left(\frac{x}{2\sqrt{\alpha_m(0.95 + 0.1\boldsymbol{\xi}_2)t}} \right). \tag{13}$$

Now, let us show how the computation of the variance and the computation of the contribution of each source of uncertainty can be reduced only to the computation of some integrals on the analytical solution shown in Eq. 13 for some fixed values of x and t:

The ANOVA functional expansion (more details are provided in the next subsection) is a unique tool for assessing the contribution of each uncertainty (and of the interactions) to the global variance. This is computed as follows (variables x and t are dropped since this does not change the following developments)

$$T(\boldsymbol{\xi}) = T_0 + T_{\xi_1} + T_{\xi_2} + T_{\xi_1\xi_2}, \tag{14}$$

where

$$
\begin{aligned}
T_0 &= \int_{\Xi^2} T(\boldsymbol{\xi}) p(\boldsymbol{\xi}) \mathrm{d}\xi; \\
T_{\xi_1} &= \int_{\Xi} T(\boldsymbol{\xi}) p(\xi_2) \mathrm{d}\xi_2 - T_0; \\
T_{\xi_2} &= \int_{\Xi} T(\boldsymbol{\xi}) p(\xi_1) \mathrm{d}\xi_1 - T_0; \\
T_{\xi_1\xi_2} &= T(\boldsymbol{\xi}) - T_{\xi_1} - T_{\xi_2} - T_0.
\end{aligned}
\tag{15}
$$

The overall variance σ^2 can be computed by means of the ANOVA expansion as

$$\sigma^2 = \sigma_{\xi_1}^2 + \sigma_{\xi_2}^2 + \sigma_{\xi_1\xi_2}^2, \tag{16}$$

where

$$
\begin{aligned}
\sigma_{\xi_1}^2 &= \int_{\Xi} T_{\xi_1}^2 p(\xi_1) \mathrm{d}\xi_1; \\
\sigma_{\xi_2}^2 &= \int_{\Xi} T_{\xi_2}^2 p(\xi_2) \mathrm{d}\xi_2; \\
\sigma_{\xi_1\xi_2}^2 &= \int_{\Xi^2} T_{\xi_1\xi_2}^2 p(\boldsymbol{\xi}) \mathrm{d}\xi.
\end{aligned}
\tag{17}
$$

Note that $\sigma_{\xi_1}^2$, $\sigma_{\xi_2}^2$ represent the unique contribution of ξ_1 and ξ_2 to the global variance σ^2, respectively. Moreover, $\sigma_{\xi_1\xi_2}^2$ represents the contribution given by the interaction between ξ_1 and ξ_2.

Note that only integrals of the expression defined in Eq. 13 are required, in order to compute the contributions to the variance for fixed values of (x, t). In Figure 3 (on the right), the solution is then represented in terms of mean and the associated error bars (square root of the variance, *i.e.* standard deviation). Figure 4 illustrates the variance of the temperature $t = 60$ s, induced by each uncertainty. Note that the contribution T_w is predominant and explains most of the global variability of the temperature. This simple example illustrates the interest in propagating some physical input uncertainties through numerical models.

3.3   Non-intrusive formulations for expensive computer codes

Unfortunately, generally, it is not possible to compute an analytical solution of the problem defined in Eq. 1. This could require the resolution of a complex system of equation, relying on a numerical approximation of the solution on some discretized grid of the numerical domain. Note then that computing the integrals of Eq. 17 can be very costly. Moreover, some additional issues
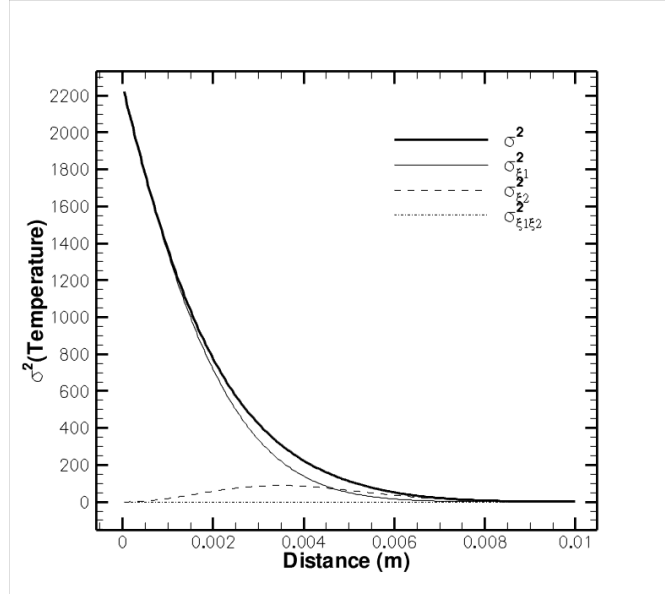
Figure 4: Variance of the temperature (including the contribution of each uncertainty) at a time of 60 seconds.

could arise in the presence of a large number of uncertainties or if the quantity of interest features some discontinuities. The real challenge is then to formulate an efficient numerical algorithm permitting to build an accurate representation of the quantity of interest as a function of input uncertainties.

As previously mentioned, only non-intrusive strategy are targeted in this work. In particular, here, we tackle a problem featuring a large number of uncertainties, that can be very challenging to solve, due to the so-called Curse of Dimensionality. It refers to the loss of convergence and the infeasible number of calculations needed when the number of parameters increases, for any chosen method. We have partially cured this problem with a two-steps approach. First, we applied an anchored-ANOVA approach on the complete problem. This analysis permits to compute the hierarchy and detect the most important uncertainties. Note that this approach only needs a very reduced number of deterministic simulations to perform uncertainty propagation and sensitivity analysis. In a second step, we applied a Polynomial-Chaos approach for treating the subspace including only the predominant parameters, in order to provide a good representation of the quantity of interest in the reduced stochastic space.

As mentioned before, due to the non-intrusivity of the stochastic methods considered here, the coupling with PATO, or any other heat and mass transfer computational model, is very straightforward: it reduces to the creation of a small interface for building automatically PATO input parameters files for each set of uncertain conditions.

Both methods are described briefly in the following. For more details, refer to [24] for the Polynomial-based method and to [25] for the anchored-ANOVA approach.

3.3.1 Anchored-ANOVA approach: Definitions and basic notions

In order to introduce the less expensive *anchored ANOVA*, the Dirac measure is used for the integrals of Eq. (9):

$$p(\boldsymbol{\xi}_i)\,\mathrm{d}\boldsymbol{\xi}_i = \delta(\boldsymbol{\xi}_i - c_i)\,\mathrm{d}\boldsymbol{\xi}_i \quad \text{for} \quad i = 1, \cdots, N \tag{18}$$

Thus, $p(\boldsymbol{\xi})\,\mathrm{d}\boldsymbol{\xi} = \delta(\boldsymbol{\xi} - \mathbf{c})\,\mathrm{d}\boldsymbol{\xi}$. The point $\mathbf{c} = (c_1, \cdots, c_N)$ is called "anchor point". Hence, the ANOVA component terms in Eq. (9) can be expressed as follows:

$$
\begin{aligned}
\phi(\mathbf{c}) &= \phi_0 \\
\phi(\mathbf{c}|\boldsymbol{\xi}_i) &= \phi_0 + \phi_i(\boldsymbol{\xi}_i) \\
\phi(\mathbf{c}|\boldsymbol{\xi}_i, \boldsymbol{\xi}_j) &= \phi_0 + \phi_i(\boldsymbol{\xi}_i) + \phi_j(\boldsymbol{\xi}_j) + \phi_{ij}(\boldsymbol{\xi}_i, \boldsymbol{\xi}_j) \\
\vdots
\end{aligned}
\tag{19}
$$

The formulae in Eq. (19) are used to quantify the expectation and variance of the component functions, by simply evaluating the model outputs at chosen sampling points. For more details, see [25]. This permits a strong reduction of the computational cost, since this avoids the computation of several integrals. Moreover, a variance-based adaptive criterion (see for more details [26]) is used in order to compute the so-called effective dimension and to evaluate high-order interactions with a reduced computational cost. The order at which the ANOVA model is truncated, is called effective dimension, beyond which the difference between the ANOVA model and the truncated expansion in a certain measure is very small. This implies that we will ignore terms in the ANOVA model corresponding to interactions exceeding the fixed threshold.

In this work, a covariance decomposition of the output variance has been considered, as proposed in [25], in order to accurately compute the statistics using the anchored-ANOVA expansion. The covariance decomposition makes the result less sensitive to the choice of the anchor point if a full expansion of the anchored ANOVA is employed.

3.3.2 Polynomial-chaos based approach

Under specific conditions, a stochastic process can be expressed as a spectral expansion based on suitable orthogonal polynomials, with weights associated to a particular probability density function. The first study in this field is the Wiener (1938) process. The basic idea is to project the variables of the problem onto a stochastic space spanned by a complete set of orthogonal polynomials Ψ that are functions of random variables $\boldsymbol{\xi}$. For example, the unknown variable ϕ has the following spectral representation:

$$\phi(\boldsymbol{\xi}) = \sum_{i=0}^{\infty} \phi_i \Psi_i(\boldsymbol{\xi})). \tag{20}$$

In practice, the series in Eq. (20) has to be truncated in terms of the polynomial degree p_0, where the total number of terms of the series M is determined by:

$$M + 1 = \frac{(N + p_0)!}{N!\, p_0!}, \tag{21}$$

where N is the dimensionality of the uncertainty vector $\boldsymbol{\xi}$. Each polynomial $\Psi_i(\boldsymbol{\xi})$ is a multivariate polynomial form which involves tensorization of 1D polynomial forms. The polynomial basis is chosen accordingly to the Wiener-Askey scheme [27] in order to select orthogonal polynomials

with respect to the probability density function $p(\boldsymbol{\xi})$ of the input. The orthogonality can be advantageously used to compute the coefficients of the expansion in a non-intrusive PC framework

$$\phi_i = \frac{\langle \phi(\boldsymbol{\xi}), \Psi_i(\boldsymbol{\xi}) \rangle}{\langle \Psi_i(\boldsymbol{\xi}), \Psi_i(\boldsymbol{\xi}) \rangle}, \quad \forall i. \tag{22}$$

Several approaches can be used to estimate PC coefficients. The approach used in this study is based on quadrature formula. As a consequence, the solution of a deterministic problem for each quadrature point is required.

For further details, see Congedo *et al.*[24]. In both cases, once the chaos polynomials and the associated ϕ_i coefficients are computed, the expected value and the variance of the stochastic solution $\phi_i(\boldsymbol{\xi})$ are obtained from:

$$E_{PC} = \phi_0 \tag{23}$$

$$Var_{PC} = \sum_{i=1}^{N} \phi_i^2 \langle \Psi_i^2 \rangle \tag{24}$$

Another interesting property of PC expansion is to make easier sensitivity analysis based on the analysis of variance decomposition (ANOVA). It can be easily computed by using some interesting properties of the previous development [28]. Let us recall here that the contribution to the variance of a given random variables with index k, *i.e.* the first order Sobol's index, can be obtained by:

$$S_k = \frac{\sum_{i \in \alpha} \phi_i^2 \langle \Psi_i^2(\boldsymbol{\xi}) \rangle}{Var_{PC}} \tag{25}$$

where α represent the set of indexes associated to a given uncertainty k. For more details, Ref. [28] is strongly recommended.

4   Results

The Anchored-ANOVA method is applied to the problem presented in section 2. We present first the convergence analysis with respect to the number of samples considered to get well-converged statistics of all the quantities of interest. In Anchored-ANOVA, the first-order analysis is based on a chosen number of points per direction. We have reported in Table 1 the outcome of this analysis for the temperature computed at a depth of 1.5 cm at a time equal to $80s$, in terms of decreasing contributions to the variance, for eight and sixteen points along each direction, respectively (which makes a total number of runs of the solver of 216 and 432, respectively). As it can be observed, errors are quite small, indicating that quantities are converged with only eight points per direction. Same conclusions can be drawn for all the other quantities of interest considered in this work, *i.e.* temperatures at different depths, the virgin front and the char front. Results shown in the following rely then on this analysis.

Let us now analyse the results from a quantitative and qualitative point of view. Figure 5 presents the transformation of the ablative material with error bars, which represent the spreading of the quantities of interest in terms of standard deviation. The plotted results are the surface recession - due to ablation - and the propagation of the pyrolysis front. The char 2% and virgin 98% are used in the ablation community to identify almost completely charred material (2% left of virgin matrix) and almost pristine virgin material (98% left of virgin matrix). The charring zone is considered to be between these two accepted limits [16]. Note that, since the heating is quite soft at the beginning of the simulation, the material is fully pyrolysed before being ablated. This explains why the char 2% and the wall curves are clearly separated in this

Table 1: Contribution to the variance of each uncertainty and error analysis with respect to the number of points per direction. Absolute and relative differences are also given.

Unc.	Contrib. q16 (%)	Contrib. q8 (%)	Δ_{abs}	Δ_{rel}
24	16.9	16.9	0.0	0.0
3	14.8	14.8	0.0	0.0
4	14.7	14.8	0.1	$6.8 \cdot 10^{-3}$
26	9.03	9.01	0.02	$2.2 \cdot 10^{-3}$
1	8.31	8.32	0.01	$1.2 \cdot 10^{-3}$
2	8.29	8.3	0.01	$1.2 \cdot 10^{-3}$
9	7.63	7.64	0.01	$1.3 \cdot 10^{-3}$
11	5.13	5.13	0.0	0.0
22	4.05	4.05	0.0	0.0
8	2.88	2.88	0.0	0.0
14	2.88	2.88	0.0	0.0
12	2.48	2.48	0.0	0.0
15	1.48	1.48	0.0	0.0
7	1.15	1.15	0.0	0.0
16	0.166	0.166	0.0	0.0
18	$5.05 \cdot 10^{-2}$	$5.03 \cdot 10^{-2}$	$0.2 \cdot 10^{-3}$	$4.0 \cdot 10^{-3}$
10	$3.78 \cdot 10^{-2}$	$3.78 \cdot 10^{-2}$	0.0	0.0
13	$5.81 \cdot 10^{-3}$	$5.81 \cdot 10^{-3}$	0.0	0.0
20	$6.68 \cdot 10^{-4}$	$6.7 \cdot 10^{-4}$	$0.2 \cdot 10^{-5}$	$3.0 \cdot 10^{-3}$
6	$7.22 \cdot 10^{-5}$	$7.21 \cdot 10^{-5}$	$0.1 \cdot 10^{-6}$	$1.4 \cdot 10^{-3}$
5	$1.01 \cdot 10^{-5}$	$1.04 \cdot 10^{-5}$	$0.3 \cdot 10^{-6}$	$3.0 \cdot 10^{-2}$
17	0.0	0.0	0.0	0.0
19	0.0	0.0	0.0	0.0
21	0.0	0.0	0.0	0.0
23	0.0	0.0	0.0	0.0
25	0.0	0.0	0.0	0.0
27	0.0	0.0	0.0	0.0

case. The observed variability is very small for the three curves. In fact, for the virgin 98%, which is the worst case, the Coefficient of Variation (standard deviation to mean ratio) is of the order of 3%.

A physical analysis of the results is now presented in terms of the contribution of each uncertainty to several quantities, namely the recession, the virgin front, the char front and the surface temperature, as a function of time. The results are presented in Figure 6. The uncertainties propagated on the material properties are in agreements with previous studies [6, 5, 22]. Concerning the recession and the location of the Char 2%, the maximal standard deviation is of the order of 0.03-0.04 cm. As it can be observed in Figure 6a and b, the location of the recession and char 2% mostly depend on both the parameters influencing the heat transfer in the charred material and the pyrolysis parameters. The virgin 98% is predominantly influenced by the uncertainty on the Activation energy 1, which controls the initiation of pyrolysis. Finally, the surface temperature is mostly driven by the char's emissivity except at the start of the pyrolysis reaction, where the activation energies and gas composition are predominant.

We would like to point out a new result. The uncertainty on the elemental pyrolysis gas composition (Carbon, Hydrogen and Oxygen) clearly induces variability on the studied quantities. The effect of the these uncertainties is observed on the in-depth temperature evolution as well, as shown in Figure 7, where the contributions of each uncertainty to the variance of the temperature is computed over the time at different depths in the material. The standard deviation of the temperature takes the highest value at a depth of 0.7 cm (100 K), while it remains quite small for the other depths considered here.

With the advancement of the ablation front, contributions of the virgin's parameters are quickly overtaken by char's ones. Parameters of the pyrolysis reaction and material composition also show decreasing contributions as the pyrolysis reaction comes to an end.
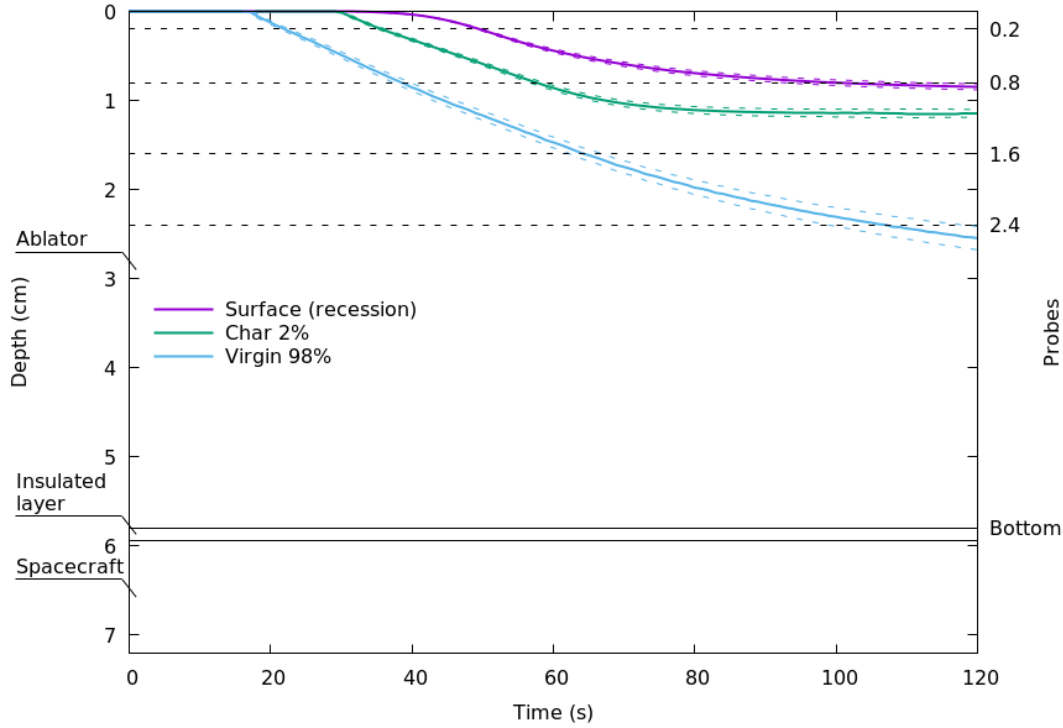
Figure 5: Recession, char at 2% and virgin at 98% with the $\pm$ standard deviation envelope.

In order to make more evident the different contributions, Figure 8 illustrates the different contributions gathered in terms of different groups of uncertainty, *i.e.* fibers and matrices properties, TACOT's composition, pyrolysis parameters, etc.

By using the low-cost sensitivity analysis technique, the hierarchy of the most important uncertain parameters contributing to the variance of the temperature can be computed as a function of the depths at a fixed time. For example, in Figure 9 we show the hierarchy at a time of 80 s. As it can be observed, the trend is highly non linear, and this could be particularly useful to build reliable design margin policies and to guide material model development efforts.

4.1 Construction of the Polynomial-Chaos based surrogate

As explained in Section 3.3.2, the interest of low-cost sensitivity analysis technique is twofold. More than only identifying a ranking of main uncertainties, it can be used in order to build a surrogate model (a Polynomial-Chaos based one in this case) on a reduced set of uncertainties, *i.e.* the predominant ones. This is applied here to the temperature computed at a depth of 1.6 cm for different times. Note that this can be easily applied to a whatever quantity of interest, but the surrogate will be not the same since the most important uncertainties can be different with respect to the time, the depth and the quantity of interest.

In the case under consideration, first the uncertainties contributing the most to the variance of the temperature at different times are computed (Figure 10 illustrates the ranking for a time $t = 80$ s where the variance is maximal).

(a) Recession

(b) Char 2% location
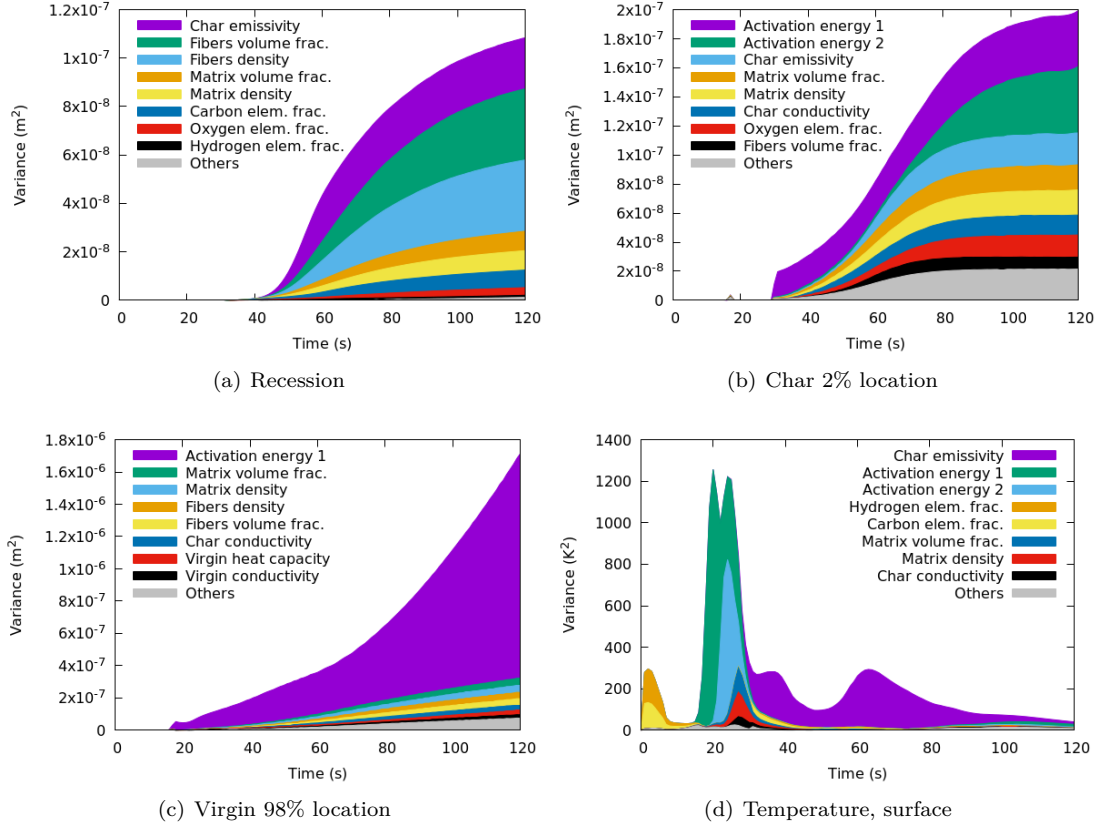
(c) Virgin 98% location

(d) Temperature, surface

Figure 6: Total variance divided by contributor, computed for several quantities, as a function of time.

Secondly, the PC-based surrogate is constructed on a set of input parameters defined by the predominant uncertainties. Here, uncertainties labeled as 24, 3, 4, 26, 1, 2, 9, 11 and 22 are chosen as input parameters (See Section 2.2 for identifying each uncertainty).

Obviously, the reduction of the problem yields a loss of accuracy with respect to the statistics computation, which could be estimated. Variance reduction is around 11%, which is mainly due to the high number of significant parameters, which are neglected in the reduced problem.

Using the surrogate model, a whatever post-processing statistical analysis can be done for free. As an example, the Probability Density Function (PDF) of the temperature at different times are computed and represented in Figure 11. As it can be observed, gaussian-like PDF can be observed.

One can see here an efficient method for studying TPS response under uncertainties.

5   Conclusion

The objective of the study was to propagate both material and pyrolysis gas composition uncertainties on the thermal response of the TPS of a spacecraft during atmospheric entry. We chose to study the entry of Stardust that was the first mission using the new generation of
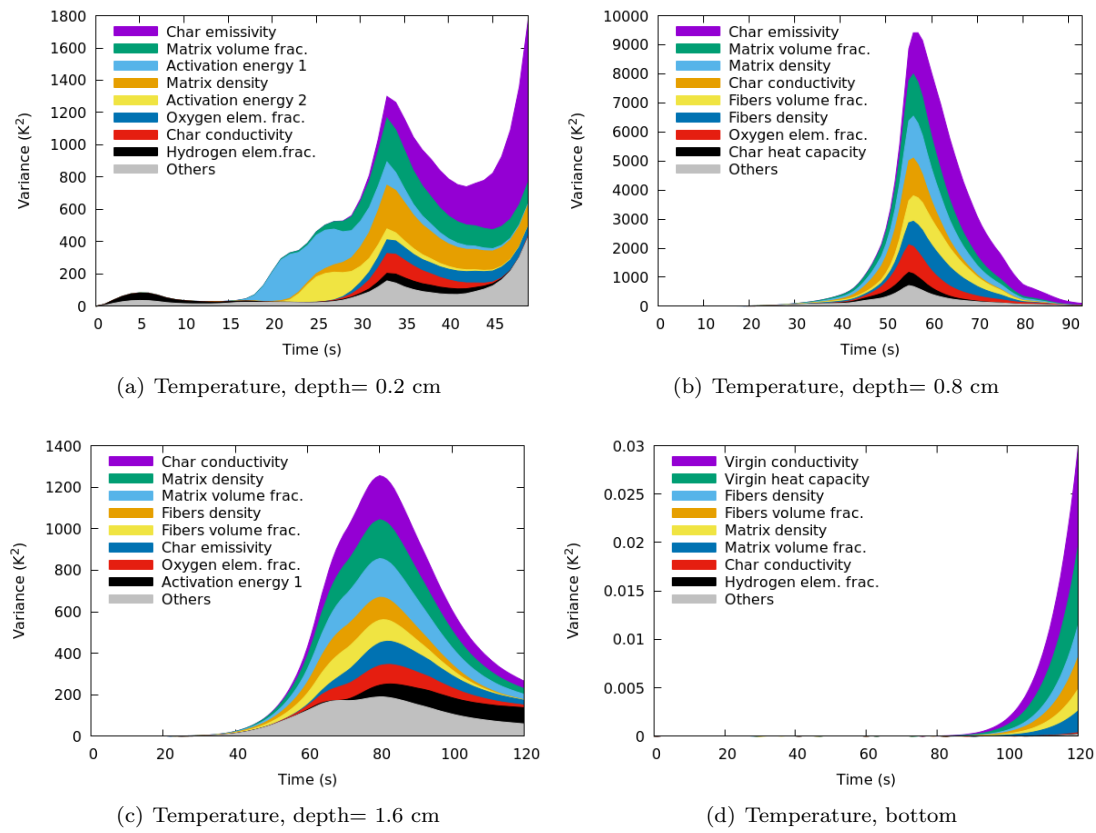
(a) Temperature, depth= 0.2 cm

(b) Temperature, depth= 0.8 cm

(c) Temperature, depth= 1.6 cm

(d) Temperature, bottom

Figure 7: Total variance divided by contributor, computed for several quantities, as a function of time.

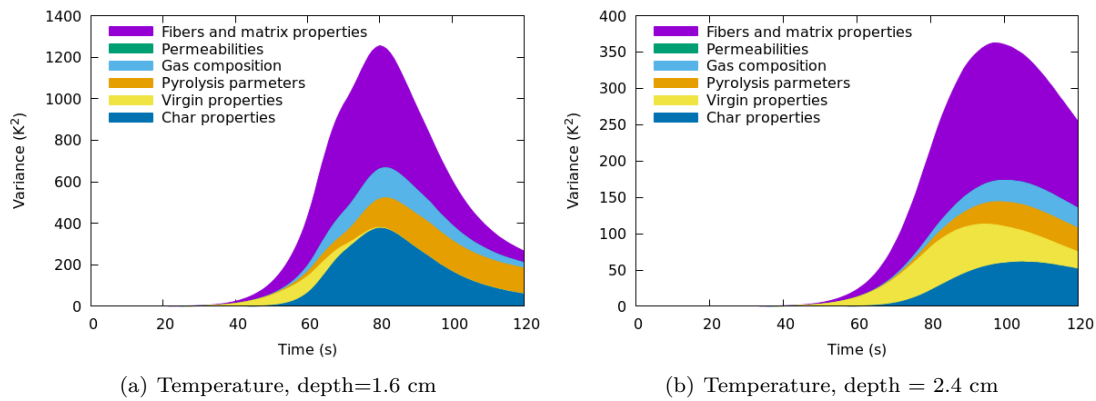(a) Temperature, depth=1.6 cm

(b) Temperature, depth = 2.4 cm

Figure 8: Total variance divided by contributor, computed for several quantities, as a function of time. Here, uncertainties are classified into different groups.
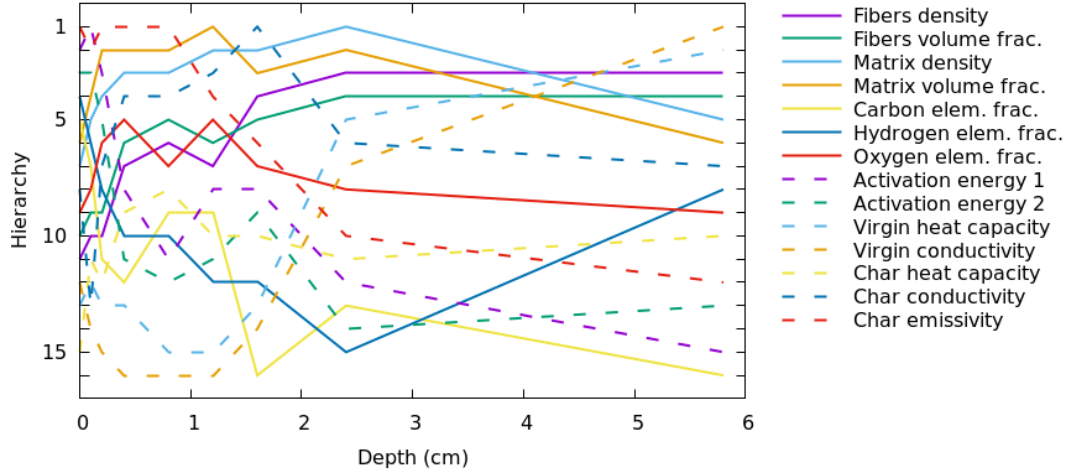
Figure 9: Hierarchy of the most relevant uncertain parameters to the temperature variance (sorted: the higher, the bigger Sobol index) as a function of depth at t=80 s.
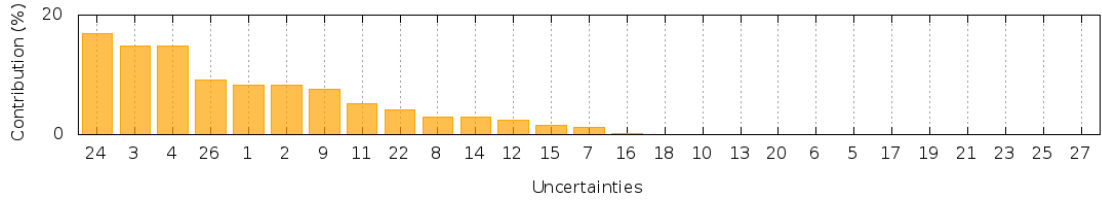

Figure 10: Sorted contributions at a depth of 1.6 cm and at a time of $t = 80$ s

low-density carbon-phenolic ablators. Due to the high computational cost of varying pyrolysis gas composition, a low-cost sensitivity analysis technique based on ANOVA has been used. To clearly explicit the method in the field of material analysis, analytical derivations of the ANOVA method were presented in the case of a well known deterministic heat transfer problem - transient conduction in a solid. Then, a sensitivity analysis technique based on anchored-ANOVA was presented, permitting to treat problems described by expensive computed codes with several uncertainties. This technique has been interfaced with PATO, a reactive porous material analysis code distributed Open Source by NASA (https://software.nasa.gov/software/ARC-16680-1A, retrieve 26/06/2018). The suite of tools have been shown to be efficient to propagate uncertainties and to successfully provide parameter hierarchies in the case of complicated simulations. The clear contribution of uncertainties of pyrolysis gas composition has been revealed for the first time. Perspectives of this work consist in using the suite of tool for inverse problems, e.g. use optimization under uncertainties to optimize material properties for targeted conditions.
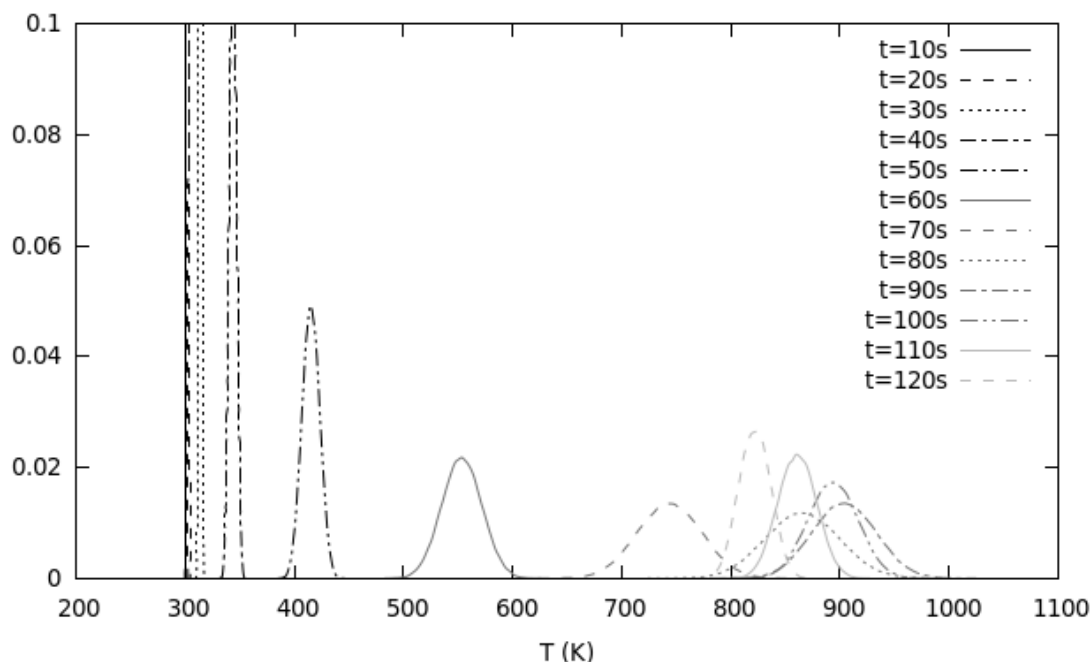
Figure 11: PDF of the temperature at a depth of 1.6 cm at different times.

References

[1] J. D. Anderson, Hypersonic and high temperature gas dynamics, Mac Graw-Hill, New-York, 1989.

[2] G. Duffa, Ablative Thermal Protection Systems Modeling, AIAA Education Series, 2013. `doi:10.2514/4.101717`.

[3] M. Stackpoole, S. Sepka, I. Cozmuta, D. Kontinos, Post-flight evaluation of stardust sample return capsule forebody heatshield material, AIAA paper 1202 (2008) 1–7.

[4] J. Lachaud, T. van Eekelen, J. B. Scoggins, T. E. Magin, N. N. Mansour, Detailed chemical equilibrium model for porous ablative materials, International Journal of Heat and Mass Transfer 90 (2015) 1034–1045, doi:10.1016/j.ijheatmasstransfer.2015.05.106.

[5] M. J. Wright, R. Beck, K. Edquist, D. Driver, S. Sepka, E. Slimko, W. Willcockson, Sizing and margins assessment of the mars science laboratory aeroshell thermal protection system, Journal of Spacecraft and Rockets 51 (4) (2014) 1125–1138.

[6] S. A. Sepka, M. J. Wright, Monte carlo approach to fiat uncertainties with applications for mars science laboratory, Journal of Thermophysics and Heat Transfer 25 (2011) 516–522. `doi:10.2514/1.49804`.

[7] S. A. Sepka, M. K. McGuire, J. V. Kam, A reliability comparison of classical and stochastic thickness margin approaches for the orion heat shield resulting from material property uncertainties, AIAA paper 1480. `doi:10.2514/6.2018-1480`.

[8] H.-W. Wong, J. Peck, R. Bonomi, J. Assif, G. Reinisch, J. Lachaud, N. N. Mansour, Quantitative determination of species production from the pyrolysis of a phenol-formaldehyde resin, Polymer Degradation and Stability 112 (2015) 122–131.

[9] B. K. Bessire, S. A. Lahankar, T. K. Minton, Pyrolysis of phenolic impregnated carbon ablator (pica), Applied Materials and Interfaces 3 (7) (2015) 1383–1395.

[10] H.-W. Wong, J. Peck, J. Assif, F. Panerai, J. Lachaud, N. N. Mansour, Detailed analysis of species production from the pyrolysis of phenolic impregnated carbon ablator., Journal of Analytical and Applied Pyrolysis 122 (2016) 258–267.

[11] N. Fajraoui, M. Fahs, A. Younes, B. Sudret, Analyzing natural convection in porous enclosure with polynomial chaos expansions: Effect of thermal dispersion, anisotropic permeability and heterogeneity, International Journal of Heat and Mass Transfer 115 (2017) 205 – 224.

[12] X. Wang, C. Yan, S. Ju, Y. Zheng, J. Yu, Uncertainty analysis of laminar and turbulent aeroheating predictions for mars entry, International Journal of Heat and Mass Transfer 112 (2017) 533 – 543.

[13] A. Turchi, P. M. Congedo, T. E. Magin, Thermochemical ablation modeling forward uncertainty analysis-part i: Numerical methods and effect of model parameters, International Journal of Thermal Sciences 118 (2017) 497 – 509.

[14] A. Turchi, P. M. Congedo, B. Helber, T. E. Magin, Thermochemical ablation modeling forward uncertainty analysis-part ii: Application to plasma wind-tunnel testing, International Journal of Thermal Sciences 118 (2017) 510 – 517.

[15] K. A. Trumble, I. Cozmuta, S. Sepka, P. Jenniskens, Post-flight aerothermal analysis of the stardust sample return capsule, AIAA paper 1201 (2008) 1–15.

[16] J. Lachaud, A. Martin, T. van Eekelen, I. Cozmuta, Ablation test-case series #2, version 2.8, Jan. 2011, 8 p., prepared for the 5th Ablation Workshop, Feb. 28-March. 1, Lexington, Kentucky.

[17] J. Lachaud, J. B. Scoggins, T. E. Magin, M. G. Meyer, N. N. Mansour, A generic local thermal equilibrium model for porous reactive materials submitted to high temperatures, International Journal of Heat and Mass Transfer 108 (2017) 1406–1417.

[18] H. Jasak, Error analysis and estimation for the finite volume method with applications to fluid flows, Ph.D. thesis, Imperial College London (University of London) (1996).

[19] H. G. Weller, G. Tabor, H. Jasak, C. Fureby, A tensorial approach to computational continuum mechanics using object-oriented techniques, Computers in physics 12 (6) (1998) 620–631.

[20] J. Lachaud, N. N. Mansour, Porous material analysis toolbox based on openfoam and applications, Journal of Thermophysics and Heat Transfer 28 (2) (2014) 191–202, doi: 10.2514/1.T4262.

[21] A. Omidy, F. Panerai, J. Lachaud, N. N. Mansour, I. Cozmuta, A. Martin, Code-to-code comparison, and material response modeling of Stardust and MSL using PATO and FIAT, NASA CR 218960 (2015) 1–36.

[22] M. Mahzari, I. Cozmuta, I. Clark, R. Braun, An inverse parameter estimation methodology for the analysis of aeroheating and thermal protection system experimental data, AIAA paper 4027.

[23] G. E. B. Archer, A. Saltelli, I. M. Sobol', Sensitivity measures, anova-like techniques and the use of bootstrap, Journal of Statistical Computation and Simulation 58 (1997) 99–120.

[24] P. M. Congedo, C. Corre, J.-M. Martinez, Shape optimization of an airfoil in a bzt flow with multiple-source uncertainties, Computer Methods in Applied Mechanics and Engineering 200 (1) (2011) 216–232.

[25] K. Tang, P. M. Congedo, R. Abgrall, Sensitivity analysis using anchored anova expansion and high-order moments computation, International Journal for Numerical Methods in Engineering 102 (9) (2015) 1554–1584.

[26] X. Yang, M. Choi, G. Lin, G. Karniadakis, Adaptive {ANOVA} decomposition of stochastic incompressible and compressible flows, Journal of Computational Physics 231 (4) (2012) 1587 – 1614.

[27] D. Xiu, G. E. Karniadakis, The Wiener–Askey Polynomial Chaos for Stochastic Differential Equations, SIAM Journal on Scientific Computing 24 (2) (2002) 619–644.

[28] T. Crestaux, O. P. Le Maître, J. M. Martinez, Polynomial chaos expansion for sensitivity analysis, Reliability engineering and system safety **94** (7) (2009) 1161 – 1172.

Appendix A

Detailed demonstrations of the analytical resolution of the transient heat transfer equation given by

$$\partial_{\mathbf{t}} T - \alpha \, \partial_{\mathbf{x}}^{\mathbf{2}} T = 0, \tag{26}$$

where α is a constant diffusivity, appears to be hard to find in text books. We will present its resolution using the Laplace transform for a semi-infinite unidimensional medium, with the following boundary conditions

- $T(\forall x, t < 0) = T_0$

- $T(x = 0, t \geqslant 0) = T_w$

corresponding to a homogeneous medium for which the surface temperature is suddenly raised. Let us apply a variable change that will simplify the integration: $\theta(x, t) = T(x, t) - T_0$. Applying the change of variable and the Laplace transform, Eq. 26 rewrites

$$\int_0^\infty e^{-st} \partial_x^2 \theta \, dt - \frac{1}{\alpha} \int_0^\infty e^{-st} \partial_t \theta \, dt = 0 \tag{27}$$

In the Laplace space, the variable is defined as $\theta^* = \int_0^\infty e^{-st} \theta \, dt$. After permutation (between $\int_0^\infty \cdot$ and $\partial_x^2 \cdot$) and integration of the first integral, we obtain

$$\partial_x^2 \theta^*(x) - \frac{1}{\alpha} [s \, \theta^*(x) - \theta(x, 0)] = 0 \tag{28}$$

Thanks to the change of variable, we have $\theta(x, 0) = 0$ and Eq. 28 simplifies into

$$\partial_x^2 \theta^*(x) - \frac{s}{\alpha} \theta^*(x) = 0 \tag{29}$$

The solution of this second order ordinary differential equation is

$$\theta^*(x) = A\exp(\sqrt{s/\alpha}\,x) + B\exp(-\sqrt{s/\alpha}\,x) \tag{30}$$

where A and B are determined with the boundary conditions. On the semi-infinite domain, we have

- $A = 0$ as the temperature has to have a limit when x tends towards infinity.

- $\theta^*(x = 0) = B$. From $\theta(0,t) = T_w - T_0$, one obtains $B = (T_w - T_0)/s$ after applying Laplace transform.

Hence, we have

$$\theta^*(x) = \frac{T_w - T_0}{s}\exp(-\sqrt{s/\alpha}\,x) \tag{31}$$

Returning to the temporal space is done using the space change relation: $\exp(-a\sqrt{s})/s \Leftrightarrow 1 - erf(a/(2\sqrt{t})$, where erf is the error function. After some algebra and returning to variable T, we obtain the physical temperature profile as a function of time

$$T(x,t) = T_0 + (T_w - T_0)\left[1 - erf\left(\frac{x/\sqrt{\alpha}}{2\sqrt{t}}\right)\right] \tag{32}$$